

SPINTRONICS

Control and local measurement of the spin chemical potential in a magnetic insulator

Chunhui Du,^{1*} Toeno van der Sar,^{1*} Tony X. Zhou,^{1,2*} Pramey Upadhyaya,³ Francesco Casola,^{1,4} Huiliang Zhang,^{1,4} Mehmet C. Onbasli,^{5,6} Caroline A. Ross,⁵ Ronald L. Walsworth,^{1,4} Yaroslav Tserkovnyak,³ Amir Yacoby^{1,2†}

The spin chemical potential characterizes the tendency of spins to diffuse. Probing this quantity could provide insight into materials such as magnetic insulators and spin liquids and aid optimization of spintronic devices. Here we introduce single-spin magnetometry as a generic platform for nonperturbative, nanoscale characterization of spin chemical potentials. We experimentally realize this platform using diamond nitrogen-vacancy centers and use it to investigate magnons in a magnetic insulator, finding that the magnon chemical potential can be controlled by driving the system's ferromagnetic resonance. We introduce a symmetry-based two-fluid theory describing the underlying magnon processes, measure the local thermomagnonic torque, and illustrate the detection sensitivity using electrically controlled spin injection. Our results pave the way for nanoscale control and imaging of spin transport in mesoscopic systems.

Control and measurement of the chemical potential of a spin system can be used to explore phenomena ranging from quantum phase transitions (1, 2) to Bose-Einstein condensation (3, 4) and spin transport in gases and solid-state systems (5–11). In recent decades, a large scientific effort has focused on harnessing spin transport for low-dissipation information processing (7, 12–14). In contrast to charge, spin is not a conserved quantity and naturally decays on the nanoscale for a wide range of materials, including typical metals (15, 16), calling for a local detection technique. Compared to the centuries-old techniques for studying charge transport, methods for probing spin chemical potentials have only been developed recently, with leading methods based on the coupling between spin and charge transport (6, 13, 14, 17) and inelastic light scattering (3, 18). Here we introduce a fundamentally different approach, which uses a single sensor spin to measure the local magnetic field fluctuations generated by a thermal spin bath. This approach is nonperturbative and provides spa-

tial access to the spin chemical potential on a scale determined by the distance between the sensor spin and the system under study, opening the door to imaging spin transport phenomena

with resolutions down to the few-nanometer scale.

Because the spin chemical potential is inherently related to spin fluctuations, it can be quantitatively determined by measuring the magnetic fields generated by these fluctuations. We demonstrate this principle using the excellent magnetic field sensitivity of the $S = 1$ electronic spin associated with the nitrogen-vacancy (NV) center in diamond (19, 20). We measure the chemical potential of magnons—the elementary spin excitations of magnetic materials (12)—in a 20-nm-thick film of the magnetic insulator yttrium-iron-garnet (YIG) on a ~ 100 -nm-length scale (Fig. 1A). Our measurements reveal that the magnon chemical potential can be effectively controlled by exciting the system's ferromagnetic resonance (FMR) (Fig. 1, B and C).

Locally probing the weak magnetic fields generated by the fluctuations of a spin system requires nanometer proximity of a magnetic field sensor to the system. We ensure such proximity by positioning diamond nanobeams (21) that contain individually addressable NV centers onto the YIG surface (Fig. 1, D and E). We use a scanning confocal microscope to optically locate the NV centers and address their spin state (22, 23). A photoluminescence image (Fig. 1D) provides an overview of the system, showing an NV center (NV₁) in a nanobeam that is located within a few micrometers from the gold and platinum striplines used to excite magnons in the YIG.

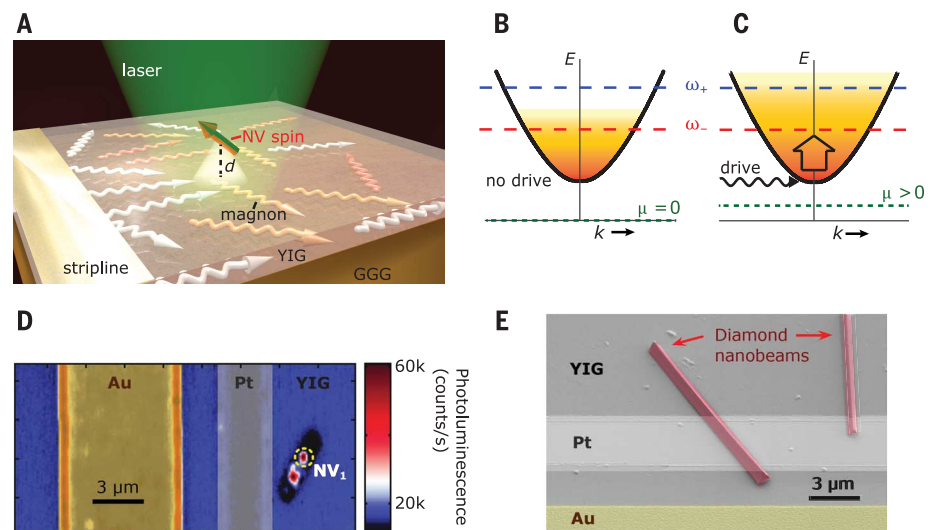


Fig. 1. Local control and measurement of the magnon chemical potential. (A) Sketch of an NV spin locally probing the magnetic fields generated by magnons in a 20-nm-thick YIG film grown on a $\text{Gd}_3\text{Ga}_5\text{O}_{12}$ (GGG) substrate. (B) Sketch of the magnon dispersion and the magnon density, which falls off as $1/\text{energy}$ ($1/E$), as indicated by the fading colors, at zero chemical potential. (C) Driving at the FMR increases the magnon chemical potential. The NV spin probes the magnon density at the NV ESR frequencies ω_{\pm} . (D) Photoluminescence image showing a diamond nanobeam containing individually addressable NV sensor spins positioned on top of the YIG film. A 600-nm-thick Au stripline (false-colored yellow) provides MW control of the magnon chemical potential and the NV spin states. A 10-nm-thick Pt stripline (false-colored gray) provides spin injection through the spin Hall effect. (E) Scanning electron microscope image of representative diamond nanobeams.

¹Department of Physics, Harvard University, 17 Oxford Street, Cambridge, MA 02138, USA. ²John A. Paulson School of Engineering and Applied Sciences, Harvard University, Cambridge, MA 02138, USA. ³Department of Physics and Astronomy, University of California, Los Angeles, 475 Portola Plaza, Los Angeles, CA 90095, USA. ⁴Harvard-Smithsonian Center for Astrophysics, 60 Garden Street, Cambridge, MA 02138, USA. ⁵Department of Materials Science and Engineering, Massachusetts Institute of Technology, 77 Massachusetts Avenue, Cambridge, MA 02139, USA. ⁶Koç University, Department of Electrical and Electronics Engineering, Sariyer, 34450 Istanbul, Turkey.

*These authors contributed equally to this work.

†Corresponding author. Email: yacoby@physics.harvard.edu

Magnons generate a characteristic magnetic field spectrum reflecting the occupation of the magnon density of states. We probe this spectrum using the sensitivity of the NV spin relaxation rates Γ_{\pm} to magnetic field fluctuations at the NV electron spin resonance (ESR) frequencies ω_{\pm} (Fig. 1, B and C) (24). For a system at thermal equilibrium, these rates can be expressed as (23)

$$\Gamma_{\pm}(\mu) = n(\omega_{\pm}, \mu) [D(\omega_{\pm}, \mathbf{k}) f(\mathbf{k}, d) d\mathbf{k} + \Gamma_{\pm}^0] \quad (1)$$

Here, $n(\omega, \mu) = \frac{k_B T}{\hbar\omega - \mu}$ is the Rayleigh-Jeans distribution (which is the Bose-Einstein distribution in the high temperature limit appropriate for our room-temperature measurements), μ is the chemical potential, k_B is Boltzmann's constant, T is the temperature, \hbar is the reduced Planck's constant, $D(\omega, \mathbf{k})$ is the magnon spectral density, \mathbf{k} is the magnon wave vector, $f(\mathbf{k}, d)$ is a transfer function describing the magnon-generated fields at the NV site, d is the distance of the NV to the YIG, and Γ_{\pm}^0 is an offset relaxation rate that is independent of the magnon spectrum. From Eq. 1, it is clear that, when $\Gamma_{\pm}(\mu) \gg \Gamma_{\pm}^0$, the chemical potential can be extracted in a way that is independent of many details of both sensor and system: Normalizing the relaxation rate measured at $\mu = 0$ by the relaxation rate measured at $\mu > 0$ yields

$$\mu = \hbar\omega_{\pm} \left(1 - \frac{\Gamma_{\pm}(0)}{\Gamma_{\pm}(\mu)}\right) \quad (2)$$

As a first step in gaining confidence in this procedure, we probed the magnetic-noise spectrum of the YIG film in the absence of external drive fields. We measured the NV spin relaxation rates as a function of an external magnetic field B_{ext}

applied along the NV axis [(23), fig. S4] and found excellent agreement with the model described by Eq. 1 (Fig. 2A). Qualitatively, the observed field dependence can be understood by noting the high density of magnons just above the FMR frequency, which induces a peak in the $m_s = 0 \leftrightarrow -1$ NV₁ relaxation rate when the corresponding ESR frequency crosses this region (Fig. 2B), where m_s labels the electron-spin eigenstate. A fit allows us to extract the distance of the NV to the YIG film (23). In extracting the NV relaxation rates, we assumed the direct relaxation rate between the $m_s = \pm 1$ states to be negligible, as this transition is spin forbidden and insensitive to magnetic noise.

Next, we studied the magnetic noise generated by the system under the application of a microwave (MW) drive field of amplitude B_{AC} (23) using the sensitivity of the NV photoluminescence to magnetic fields at the ESR frequencies. Fig. 2C shows the photoluminescence of NV₁ as a function of the drive frequency and B_{ext} . The straight lines result from the expected decrease in NV fluorescence when the drive frequency matches one of the NV ESR frequencies. In addition, the fluorescence decreases when the MW excitation frequency matches the calculated FMR condition of the YIG film. This effect results from an FMR-induced increase in the magnon density and associated magnetic field noise at the NV ESR frequencies (23, 25, 26). A line cut at $B_{\text{ext}} = 14.4$ mT shows a typical FMR linewidth of 8 MHz that we observe in these measurements (Fig. 2C, inset).

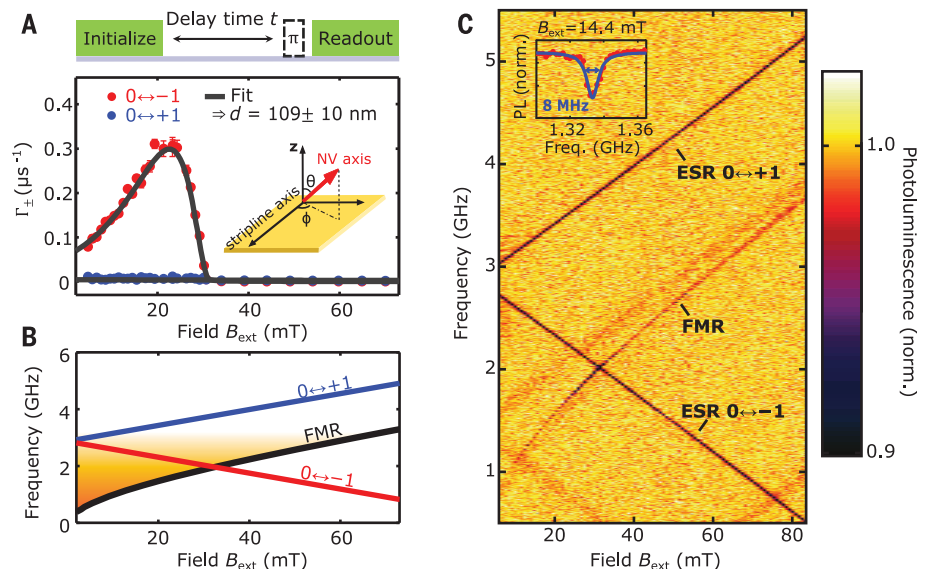
If the magnon occupation under the application of an FMR drive field can be described by the Rayleigh-Jeans distribution—as may be expected because magnon thermalization is mainly driven by the exchange interaction, which is by far the largest energy scale in our system (\sim THz)—Eq. 2

allows us to extract the chemical potential μ by measuring the NV relaxation rates. We measured the power dependence of the relaxation rate Γ_{-} of NV₁ at several values of the external magnetic field (Fig. 3A). We found that Γ_{-} increases with drive power B_{AC}^2 , consistent with the FMR-induced decrease of NV photoluminescence shown in Fig. 2C. Notably, Γ_{-} saturates as a function of drive power; moreover, the corresponding chemical potential saturates exactly at the minimum of the magnon band set by the FMR (23) (Fig. 3B). Because the band minimum is the maximum allowed value for the chemical potential of a boson system in thermal equilibrium (27), it provides a distinct reference point that is independent of any assumptions or experimentally unknown parameters. The precise match between the saturated value of the extracted chemical potential and the band minimum therefore underscores the validity of our method to extract the chemical potential. We confirmed this saturation behavior using two different NV centers over a broad range of magnetic fields (Fig. 3, B and C), providing compelling evidence that the magnon density is described by a finite chemical potential in the spectral region probed in this measurement. We independently verified that the magnon temperature increases by less than 5 K at the highest drive power used in the measurements of Fig. 3B and does not significantly influence the extracted chemical potentials [see section S6 of (23)]. Another notable feature of our data is the initial slow increase of chemical potential observed at small B_{ext} and low drive power (Fig. 3, B and D).

The build-up of chemical potential under the application of an FMR drive field can be understood as a pumping process of thermal magnons by the FMR-induced precession of the coherent

Fig. 2. Tools for characterizing the magnon chemical potential.

(A) Measured spin relaxation rates Γ_{\pm} corresponding to the $m_s = 0 \leftrightarrow \pm 1$ transitions of NV₁ as a function of an external magnetic field B_{ext} . A fit to Eq. 1 yields the distance d of NV₁ to the YIG film. The measurement sequence is depicted on top: The NV spin is prepared in the $m_s = 0$ state by using a ~ 3 - μ s green-laser pulse and left to relax for a time t . At the end of this time, we characterize the occupation probabilities of the $m_s = 0, -1$, and $+1$ states by using MW pi pulses (π) on the appropriate ESR transitions and measuring the spin-dependent photoluminescence during the first ~ 600 ns of a green-laser readout pulse. We extract Γ_{\pm} by fitting the resulting data with a three-level model, as further detailed in (23) and fig. S4. B_{ext} is applied along the axis of NV₁, at a $\theta = 65^\circ$ angle with respect to the sample-plane normal and a $\phi = 52^\circ$ in-plane angle with respect to the Au stripline (see inset). (B) Sketch of the magnon density and the NV ESR frequencies versus B_{ext} . (C) Normalized photoluminescence (PL) of NV₁ as a function of B_{ext} and the frequency of a 0.17-mT MW drive field. The labeled and unlabeled straight lines correspond to the NV ESR transitions in the electronic ground and excited states, respectively (20). Inset: Linecut showing the 8-MHz linewidth of the YIG FMR at $B_{\text{ext}} = 14.4$ mT.



spin order parameter \mathbf{sn} , where \mathbf{n} is a unit vector: An incoming thermal magnon scatters off the time-dependent \mathbf{n} , generating two thermal magnons and transferring one unit of angular momentum from the coherent spin density to the incoherent spin density \tilde{n} (23). This process is the Onsager reciprocal of a local thermomagnonic torque-induced precession of \mathbf{n} (27), which is gaining increased attention in the field of spin caloritronics. By using a two-fluid phenomenology (9), we can describe the mutual dynamics of \mathbf{n} and \tilde{n} according to the following hydrodynamic equation (23)

$$\dot{\tilde{n}} = -\frac{\tilde{\alpha}s\mu}{\hbar^2} + \eta\cos\theta_n \frac{s}{\hbar} \mathbf{z} \cdot (\dot{\mathbf{n}} \times \mathbf{n}) \quad (3)$$

Here, the first term on the right-hand side describes the decay of thermal magnons into the lattice, with $\tilde{\alpha}$ a constant related to Gilbert damping. The second term describes the pumping of thermal magnons by the FMR-induced precession of \mathbf{n} , with η parametrizing the local thermomagnonic torque between \mathbf{n} and \tilde{n} and θ_n parametrizing the instantaneous angle of \mathbf{n} with respect to the sample-plane normal \mathbf{z} . By setting $\dot{\tilde{n}} = 0$ and averaging the scalar triple product in Eq. 3 over a cycle of precession, under the assumption of the nonadiabatic pumping regime (23), we obtain

$$\mu = \kappa \frac{\eta}{\tilde{\alpha}} B_{AC}^2 \cos^2 \theta_{n_0} \quad (4)$$

where θ_{n_0} is the average magnetization angle with respect to the sample-plane normal and κ is a parameter resulting from averaging over the elliptical motion of \mathbf{n} .

A key prediction of this model, resulting from symmetry considerations (23), is that the coupling between \mathbf{n} and \tilde{n} vanishes for an in-plane orientation of the magnetization (i.e., for $\theta_{n_0} = \pi/2$). We can test this prediction by using the measurement of the chemical potential as a function of B_{ext} (Fig. 3D), as changing B_{ext} changes θ_{n_0} in a well-defined way (23). We find that the dependence of the drive efficiency $d\mu/dB_{AC}^2$ on B_{ext} in the low-power regime is accurately described by our theoretical prediction given by Eq. 4 (Fig. 3E), further supporting our conclusion that we are extracting the chemical potential correctly. We highlight that the precise knowledge of the in situ drive amplitude B_{AC} provided by our NV sensor (23) is essential for this comparison. From a fit, we extract $\eta \approx 10^{-4}$ (23), which is comparable to the measured YIG Gilbert damping parameter $\alpha \approx 10^{-4}$ (28). According to the theoretical model studied in (29), η describes the purely magnonic contribution to Gilbert damping and may thus be expected to be bounded by α . The comparability of η and α suggests that thermal magnons can exert a torque large enough to induce a magnetization precession.

Finally, we illustrated the power of our technique by characterizing the chemical potential that results from electrically controlled spin injection via the spin Hall effect (SHE). The SHE is a phenomenon originating from spin-orbit inter-

action, in which a charge current generates a transverse spin current. Such a spin current can be injected into a magnetic system, a technique widely used to study nonequilibrium magnon properties (14, 15, 17, 30, 31). Fig. 4A shows the measured relaxation rate of NV_1 , located $\sim 1.7 \mu\text{m}$ from the edge of the Pt stripline (Fig. 1D), as a function of the electrical current density J_c in the Pt. We observed a clearly asymmetric dependence that is well described by a second-order polynomial (blue solid line)

$$\Gamma_-(\mu) = \Gamma_-(0) + \Gamma_1 + \Gamma_2 \quad (5)$$

with $\Gamma_1 \propto J_c$ the linear part and $\Gamma_2 \propto J_c^2$ the quadratic part.

Intuitively, we may expect the quadratic part of this polynomial to result from heating due to Ohmic dissipation in the Pt wire and the linear part to result from the SHE. We checked this expectation by exploiting the capability of the NV sensor to determine the temperature at the NV site through measurements of changes in the zero-field splitting of the NV spin states (23, 32). We assumed this temperature to be equal to the local YIG temperature because of the high thermal conductivity of diamond and the relatively insulating properties of air. We then used Eq. 1 to calculate the expected change in NV relaxation over the experimentally determined relevant temperature range of ~ 40 K (23). A comparison of this calculation with the data shows excellent quantitative agreement (Fig. 4B), illustrating the

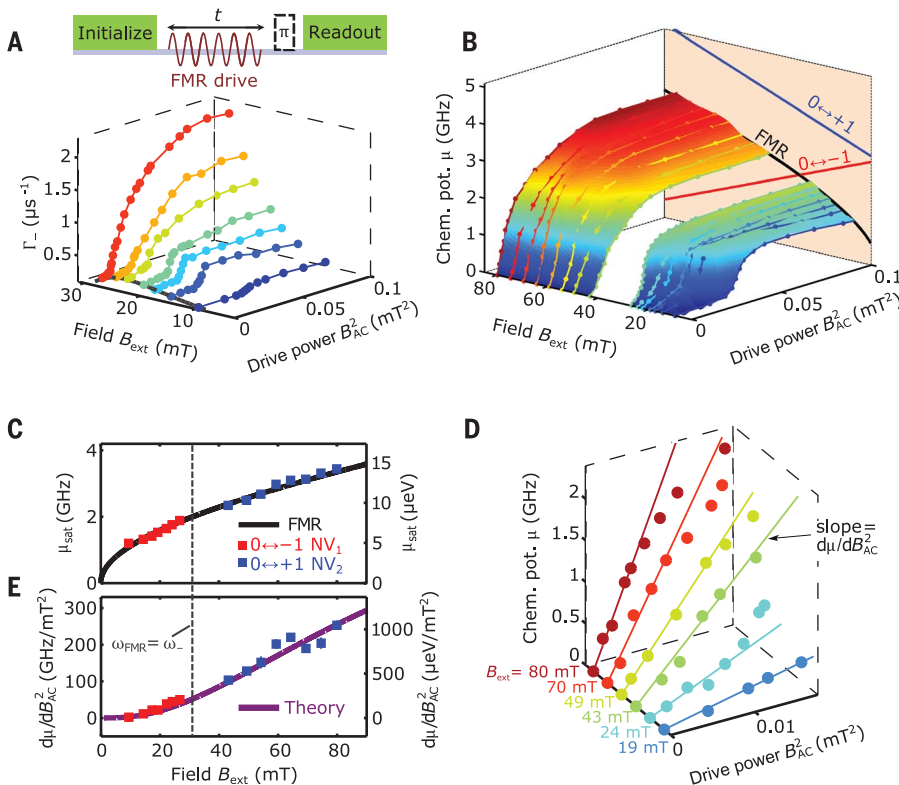


Fig. 3. Magnon chemical potential (μ) under

FMR excitation. (A) NV_1 relaxation rate Γ_- as a function of the on-chip power B_{AC}^2 of a magnetic drive field applied at the FMR frequency, for different values of B_{ext} . The gray line is the fit from Fig. 2A. Top, measurement sequence. **(B)** μ as a function of B_{AC}^2 and B_{ext} . μ saturates at the minimum of the magnon band set by the FMR frequency. **(C)** Field dependence of the saturated value of the chemical potential μ_{sat} calculated from averaging μ in the region $0.05 \text{ mT}^2 < B_{AC}^2 < 0.1 \text{ mT}^2$ [see (B)]. The black curve is the FMR. The red and blue points are measured by using the NV_1 $m_s = 0 \leftrightarrow -1$ and NV_2 $m_s = 0 \leftrightarrow +1$ transitions, respectively. B_{ext} is oriented along the NV axis, at a $\theta = 65^\circ$ angle with respect to the sample-plane normal for both NVs and a $\phi = 52^\circ$ ($\phi = 6^\circ$) in-plane angle with respect to the Au stripline for NV_1 (NV_2). The NV_2 to YIG distance is $65 \pm 10 \text{ nm}$ (23). **(D)** At low B_{AC}^2 , μ increases linearly at a rate $d\mu/dB_{AC}^2$ that depends on B_{ext} . **(E)** Field dependence of $d\mu/dB_{AC}^2$ extracted from (D). A comparison to theory yields the local thermomagnonic torque (see text). Fig. 3, A, B, and D, are shown with error bars in (23). In Fig. 3, C and E, the error bars are comparable to or smaller than the symbol size.

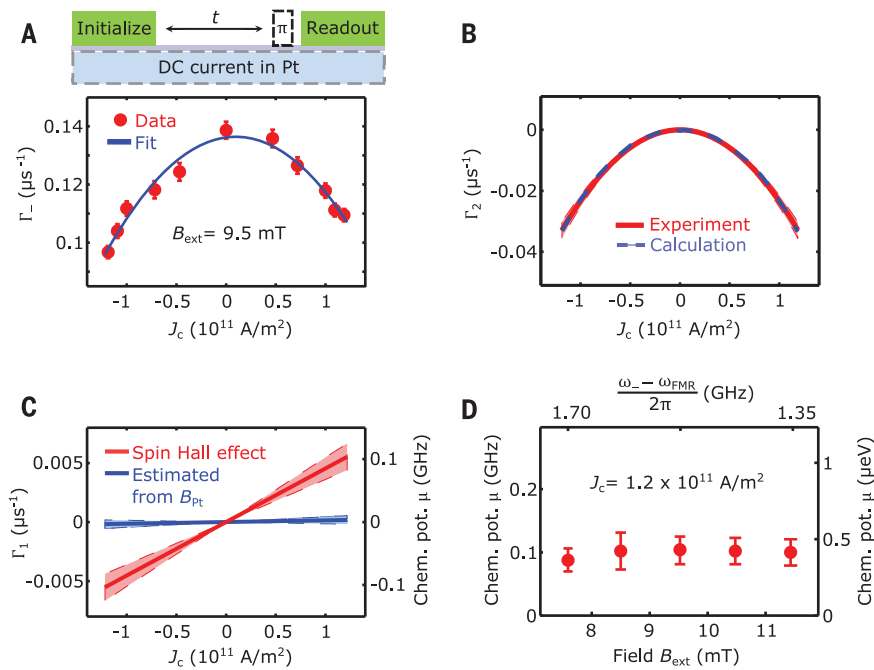


Fig. 4. Magnon chemical potential resulting from the SHE. (A) Measured NV relaxation rate Γ_- versus current density J_c in the Pt stripline. Blue curve, second-order polynomial fit. Top, measurement sequence. (B) Quadratic part of the measured change in NV relaxation rate, extracted from (A), compared to a calculation based on the experimentally determined increase in temperature resulting from Ohmic dissipation in the Pt wire. (C) Linear part of the measured change in NV relaxation rate (red line), attributed to the SHE, from which we extract the chemical potential as a function of J_c . A control measurement (23) shows that the contribution of the dc field B_{Pt} generated by the current in the Pt is negligible (blue line). (D) Field dependence of the chemical potential. In (B) and (C), the shaded regions indicate 2 SD confidence intervals based on the uncertainty of the fit parameters.

potential of NV spins for probing heat-related magnon phenomena, with applications in spin caloritronics, such as studies of the spin Seebeck effect (10, 11).

We attribute the linear part of the current-induced change in relaxation rate to a change in chemical potential induced by the SHE. Importantly, we rule out a possible influence of the Oersted field B_{Pt} generated by the current in the Pt: We first use our NV sensor to measure B_{Pt} in situ and then perform a control measurement of Γ_- as a function of an externally applied field that mimics B_{Pt} (23). We do not discern a significant effect of such a field on the NV relaxation rate (Fig. 4C). To extract the spin Hall-induced chemical potential from Γ_+ , we expand Eq. 1 in the limit $\mu \ll \hbar\omega$ and assume a linear dependence $\mu \propto J_c$ (14, 23). We find that μ increases by ~ 0.1 GHz for $J_c = 1.2 \times 10^{11}$ A/m² (Fig. 4C). Furthermore, we find that for a given current through the Pt, μ does not significantly depend on the spectral detuning between ω_- and the FMR over a ~ 0.35 -GHz frequency range, as determined by sweeping B_{ext} (Fig. 4D). In Fig. 4D, the spin-current injection efficiency is essentially constant, as the magnetization angle varies by less than 0.6° (23).

Our results show that exciting the FMR provides an efficient mechanism to control the magnon

chemical potential. Confined magnon resonances such as edge modes in ferromagnetic strips could serve as local sources of spin chemical potential to control spin currents. The ability to measure spin chemical potentials with an ultimate imaging resolution set by the NV-to-sample distance opens up new possibilities for measuring spin density, currents, and conductance in mesoscopic spin systems; exploring diffusive and ballistic spin transport; and aiding the development of new spintronic nanodevices.

REFERENCES AND NOTES

- M. W. Zwierlein, A. Schiroztek, C. H. Schunck, W. Ketterle, *Science* **311**, 492–496 (2006).
- S. Sachdev, *Quantum Phase Transitions* (Cambridge Univ. Press, ed. 2, 2011).
- S. O. Demokritov *et al.*, *Nature* **443**, 430–433 (2006).
- S. A. Bender, R. A. Duine, Y. Tserkovnyak, *Phys. Rev. Lett.* **108**, 246601 (2012).
- A. Sommer, M. Ku, G. Roati, M. W. Zwierlein, *Nature* **472**, 201–204 (2011).
- F. J. Jedema, A. T. Filip, B. J. van Wees, *Nature* **410**, 345–348 (2001).
- B. Dlubak *et al.*, *Nat. Phys.* **8**, 557–561 (2012).
- Y. Fukuma *et al.*, *Nat. Mater.* **10**, 527–531 (2011).
- B. Flebus, S. A. Bender, Y. Tserkovnyak, R. A. Duine, *Phys. Rev. Lett.* **116**, 117201 (2016).
- C. M. Jaworski *et al.*, *Nat. Mater.* **9**, 898–903 (2010).
- G. E. W. Bauer, E. Saitoh, B. J. van Wees, *Nat. Mater.* **11**, 391–399 (2012).
- A. V. Chumak, V. I. Vasyuchka, A. A. Serga, B. Hillebrands, *Nat. Phys.* **11**, 453–461 (2015).

- I. Žutić, J. Fabian, S. Das Sarma, *Rev. Mod. Phys.* **76**, 323–410 (2004).
- L. J. Cornelissen, J. Liu, R. A. Duine, J. B. Youssef, B. J. van Wees, *Nat. Phys.* **11**, 1022–1026 (2015).
- J. Sinova, S. O. Valenzuela, J. Wunderlich, C. H. Back, T. Jungwirth, *Rev. Mod. Phys.* **87**, 1213–1260 (2015).
- J. Bass, W. P. Pratt Jr., *J. Phys. Condens. Matter* **19**, 183201 (2007).
- L. J. Cornelissen, K. J. H. Peters, G. E. W. Bauer, R. A. Duine, B. J. van Wees, *Phys. Rev. B* **94**, 014412 (2016).
- S. O. Demokritov, V. E. Demidov, *IEEE Trans. Magn.* **44**, 6–12 (2008).
- J. R. Maze *et al.*, *Nature* **455**, 644–647 (2008).
- L. Rondin *et al.*, *Rep. Prog. Phys.* **77**, 056503 (2014).
- M. J. Burek *et al.*, *Nano Lett.* **12**, 6084–6089 (2012).
- A. Gruber *et al.*, *Science* **276**, 2012–2014 (1997).
- Materials and methods are available as supplementary materials.
- T. van der Sar, F. Casola, R. Walsworth, A. Yacoby, *Nat. Commun.* **6**, 7886 (2015).
- C. S. Wolfe *et al.*, *Phys. Rev. B* **89**, 180406 (2014).
- M. R. Page *et al.*, arXiv:1607.07485 [cond-mat.mes-hall] (2016).
- S. A. Bender, Y. Tserkovnyak, *Phys. Rev. B* **93**, 064418 (2016).
- M. C. Onbasli *et al.*, *APL Mater.* **2**, 106102 (2014).
- B. Flebus, P. Upadhyaya, R. A. Duine, Y. Tserkovnyak, *Phys. Rev. B* **94**, 214428 (2016).
- M. Collet *et al.*, *Nat. Commun.* **7**, 10377 (2016).
- L. Liu *et al.*, *Science* **336**, 555–558 (2012).
- V. M. Acosta *et al.*, *Phys. Rev. Lett.* **104**, 070801 (2010).

ACKNOWLEDGMENTS

We thank P. Kim for providing the setup for the nanobeam transfer and M. Warner and M. Burek for help with nanobeam fabrication. This work is supported by the Gordon and Betty Moore Foundation's Emergent Phenomena in Quantum Systems (EPIQS) Initiative through grant GBMF4531. A.Y. and R.L.W. are also partly supported by the Multidisciplinary University Research Initiative (MURI) Qubit Enabled Imaging, Sensing, and Metrology (QuISM) project. A.Y. was also partly supported by Army Research Office grant W911NF-17-1-0023. Work at the University of California, Los Angeles, is supported by the U.S. Department of Energy (DOE), Office of Basic Energy Sciences (BES) under award no. DE-SC0012190. R.L.W. and H.Z. thank the DARPA Quantum-assisted Sensing and Readout (QuASAR) program and the Smithsonian Institution. Work at the Massachusetts Institute of Technology was supported by the Solid-State Solar-Thermal Energy Conversion Center (S3TEC), an Energy Frontier Research Center funded by DOE, Office of Science, BES under award no. DE-SC0001299/DE-FG02-09ER46577. F.C. acknowledges support from the Swiss National Science Foundation grant no. P300P2-158417. Device fabrication was performed at the Center for Nanoscale Systems (CNS), a member of the National Nanotechnology Coordinated Infrastructure Network, which is supported by the NSF under award no. 1541959. CNS is part of Harvard University. C.D. and A.Y. conceived the idea and designed the project. C.D. led the project. C.D., T.v.d.S., and A.Y. designed the measurement schemes and analyzed the data. C.D. fabricated the devices and performed the measurements. T.X.Z. built the confocal setup and contributed to the device fabrication. P.U. and Y.T. developed the theory of FMR-pumping of thermal magnons. F.C. and H.Z. proposed and fabricated the nanobeams. M.C.O. and C.A.R. provided the YIG sample. C.D., T.v.d.S., and A.Y. wrote the manuscript with the help from all coauthors. C.D., T.v.d.S., T.X.Z., P.U., Y.T., F.C., H.Z., R.L.W., and A.Y. contributed to the discussions. A.Y. supervised the project. The data that support the plots within this paper and other findings of this study are available from the corresponding author on request. The authors declare no competing financial interests.

SUPPLEMENTARY MATERIALS

www.sciencemag.org/content/357/6347/195/suppl/DC1
Materials and Methods
Supplementary Text
Figs. S1 to S11
References (33–55)

25 October 2016; accepted 9 June 2017
10.1126/science.aak9611

Control and local measurement of the spin chemical potential in a magnetic insulator

Chunhui Du, Toeno van der Sar, Tony X. Zhou, Pramey Upadhyaya, Francesco Casola, Huiliang Zhang, Mehmet C. Onbasli, Caroline A. Ross, Ronald L. Walsworth, Yaroslav Tserkovnyak and Amir Yacoby

Science **357** (6347), 195-198.
DOI: 10.1126/science.aak9611

Diamonds to the rescue

Keeping track of spin transport inside a spintronic device is challenging. Du *et al.* came up with a method involving diamond nitrogen-vacancy (NV) centers, which can act like tiny, very sensitive magnetometers. The authors placed diamond nanobeams containing the NV centers in close proximity to the sample. This allowed them to measure the spin chemical potential of spin waves—so-called magnons—with nanometer resolution in the material yttrium iron garnet. Because NV centers are also sensitive to temperature, the method may be of use in spin caloritronics.

Science, this issue p. 195

ARTICLE TOOLS

<http://science.sciencemag.org/content/357/6347/195>

SUPPLEMENTARY MATERIALS

<http://science.sciencemag.org/content/suppl/2017/07/12/357.6347.195.DC1>

REFERENCES

This article cites 49 articles, 4 of which you can access for free
<http://science.sciencemag.org/content/357/6347/195#BIBL>

PERMISSIONS

<http://www.sciencemag.org/help/reprints-and-permissions>

Use of this article is subject to the [Terms of Service](#)